Original scientific paper

Informacije MIDEM
Journal of Microelectronics,
Electronic Components and Materials
Vol. 45, No. 2 (2015), 132 – 141

The optimal useful measurement range of an inductive displacement sensor

Snežana M. Djurić, Nikola M. Djurić, Mirjana S. Damnjanović

Faculty of Technical Sciences, University of Novi Sad, Serbia

Abstract: The purpose of this paper is to find the optimal useful measurement range of an inductive displacement sensor with meander type coils. The optimal useful measurement range was numerically examined using a developed model for impedance calculation. The sensor is composed of two sensor elements, with meander-type inductive coils. Each coil has five turns. With these two sensor elements, it is possible to detect normal displacement (using only one sensor element) and tangential displacement (using both sensor elements). Numerical results showed that the optimal useful measurement range was obtained when the gap of 0.23 mm was inserted in one of the coils of sensor element detecting normal displacement. Experimental results confirmed theoretical predictions. The paper demonstrates developing of a model for impedance calculation of an inductive displacement sensor. With this model, it was possible to determine numerically the optimal useful measurement range of the sensor.

Keywords: inductive coils; inductance calculation; measurement range; displacement

Optimalno uporabno območje induktivnega senzorja premika

Izvleček: Namen članka je poiskati uporabno merilno območje induktivnega senzorja premika z meandrasta tuljavami. Optimalno področje je bilo numerično določeno z razvitim modelom za izračune impedanc. Senzor je sestavljen iz dveh senzorskih elementov z meandrasto tuljavo. Vsaka tuljava ima pet zavojev. S tema dvema senzorskima elementoma je mogoče zaznati običajne premike (z uporabo le enega senzorja) in tangencialne premike (pri uporabi obeh senzorjev). Numerični izračuni optimalnega merilnega območja so pri uporabi 0.23 mm reže v enem senzorju pri detekciji normalnega premika. Meritve potrjujejo teoretične izračune. V članku je predstavljen razvoj modela, ki omogoča določitev optimalnega merilnega območja senzorja.

Ključne besede: induktivne tuljave ; izračuni induktivnosti; merilno območje; premik

* *Corresponding Author's e-mail: snesko@uns.ac.rs*

1 Introduction

The planar inductive coil sensors have a large scale of application. They can be applied in the inspection of printed circuit boards using eddy-current testing (ECT) technique [1, 2, 3]. The development and comparison of different planar fluxgate magnetic sensor structures realized in PCB technology has been reported in [4]. The planar inductive sensor with planar coil and magnetic core can detect the cracks on nonmagnetic and magnetic specimens [5]. The linear displacement sensor based on the inductive concept using meander coil and pattern guide is used to detect the displacement of moving part on linear machines [6]. The effect of inductive coil shape (meander, square, and circle shape with different turn number of inductive coils) on the sensing performance of a linear displacement sensor has been analyzed in [7]. A planar inductive coil of circle shape is used in an eddy-current sensor for high resolution displacement detection with reduced temperature coefficient [8]. An eddy current senor with rectangular sensing element, printed by ink-jet technology on a flexible substrate, for displacement application, has been presented in [9]. An inductive sensor for distance measurement employs the principle of magnetic coupling between two coplanar coils [10]. Sensors, fabricated in PCB technology, with planar meander and interdigital coils in series and parallel combination, are used for measurement and monitoring of environmental parameters [11, 12].

In our previous papers [13, 14], design, modeling, and operating principle of an inductive displacement sen-

sor, with meander-type inductive coils, was presented. The sensor is composed of two sensor elements. Each sensor element presents a pair of meander coils. One sensor element detects normal displacement, whereas the other sensor element detects tangential displacement. Sensor element for normal displacement can be used independently, whereas the sensor element detecting tangential displacement is used in combination with the element detecting normal displacement. The sensor element that detects normal displacement, with inserted gap *g* in the stationary coil, is presented in Figure 1. The width of the segments in the stationary coil is w_1 = 1.52 mm, in the moving (short-circuited coil) the width of the segments is w_2 = 0.51 mm. The distance between axes of two neighboring segments is *p* = 1.78 mm and the number of turns is five. The gap width influences the useful measurement range of the sensor. The useful measurement range of the sensor is near *y* = 0 (zero position – the axes of the segments of the stationary coil are exactly above the axes of the segments of the moving coil.) In this range the input inductance of the sensor element detecting normal displacement is invariant versus tangential displacement (*y*-direction), thus the element detects only normal displacement. The goal of this paper was to examine the optimal useful measurement range of the sensor.

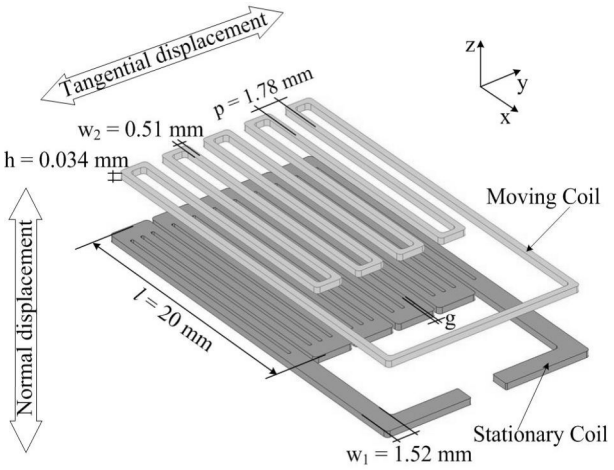

Figure 1: The sensor element, detecting normal displacement, with inserted gap in the stationary coil.

2 Model of the sensor

Each sensor element can be described with its equivalent circuit as it is shown Figure 2, where R_1 and R_2 are resistances of the stationary coil (Coil 1) and moving coil (Coil 2), L_1 and L_2 are the self-inductances of Coils 1 and 2, respectively [15].

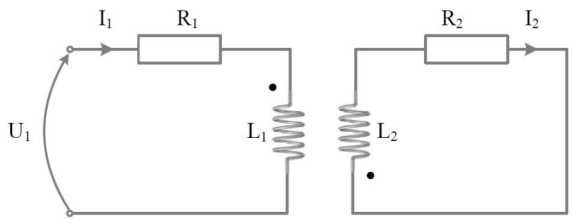

Figure 2: Equivalent electrical circuit of sensor element.

The input impedance of sensor element is equal to the input impedance of the equivalent circuit:

$$\begin{aligned} \underline{U}_1 &= R_1\underline{I}_1 + j\omega L_1\underline{I}_1 + j\omega M_{12}\underline{I}_2 \\ R_2\underline{I}_2 &+ j\omega L_2\underline{I}_2 + j\omega M_{12}\underline{I}_1 = 0 \end{aligned} \quad 2.1$$

$$\underline{I}_2 = -\frac{j\omega M_{12}}{R_2 + j\omega L_2}\underline{I}_1 \quad 2.2$$

$$\underline{U}_1 = (R_1 + j\omega L_1)\underline{I}_1 - j\omega M_{12}\frac{j\omega M_{12}}{R_2 + j\omega L_2}\underline{I}_1 \quad 2.3$$

$$\underline{Z}_{IN} = R_{IN} + j\omega L_{IN} \quad 2.4$$

where the total resistance of the impedance is

$$R_{IN} = R_1 + \frac{\omega^2 R_2 L_1 L_2 k^2}{R_2^2 + \omega^2 L_2^2} \quad 2.5$$

and the total reactance of the impedance is

$$\omega L_{IN} = \omega L_1 \frac{R_2^2 + \omega^2 L_2^2\left(1 - k^2\right)}{R_2^2 + \omega^2 L_2^2} \quad 2.6$$

Mutual position between the coils introduces magnetic coupling between coils. The coupling coefficient *k* is

$$k = \frac{M_{12}}{\sqrt{L_1 L_2}} \quad 2.7$$

where M_{12} is the mutual inductance between Coils 1 and 2, for specific mutual position, and L_1 and L_2 are the self-inductances of Coils 1 and 2, respectively. The mutual inductance changes according to displacement between Coils 1 and 2. It can be assumed that the current of conductive segments is uniformly distributed over the whole cross-section because of relatively low working frequency (1 MHz). At this relatively low frequency, the skin and proximity effects are negligible ($\delta = \sqrt{\rho_{Cu} / \pi f \mu_0}$, where ρ_{Cu} = 1.72 × 10^{-8} Ω is electrical resistivity of copper *Cu*, *f* the working frequency and $\mu_0 = 4\pi \times 10^{-7}$ H/m the permeability). The concept of the partial inductance was applied as to calculate parameters L_1, L_2 and M_{12}.

3 Inductance calculation

3.1 Self-inductance calculation of the meander-type coil with inserted gaps

In order to optimize numerically the useful measurement range of the sensor, the mathematical model that describes the influence of the gap on the self-inductance of the coil shown in Figure 3, was developed.

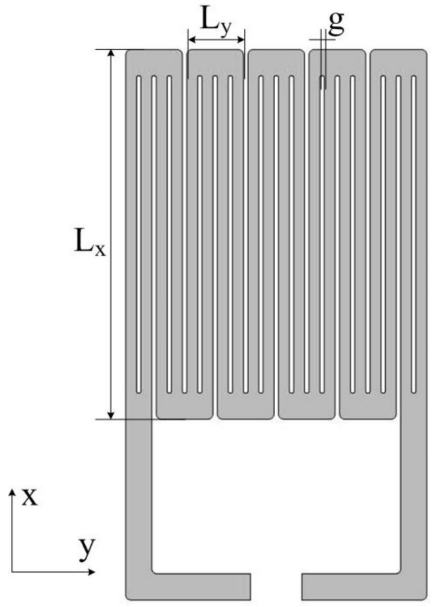

Figure 3: The stationary coil with inserted gap in conductive segments parallel to *x*-axis, l_x segments.

The equivalent circuit of the coil with inserted gaps is shown in Figure 4. The gaps were inserted symmetrically in the segments, hence it was assumed that the current in all bars was equal, and that phase shift did not change.

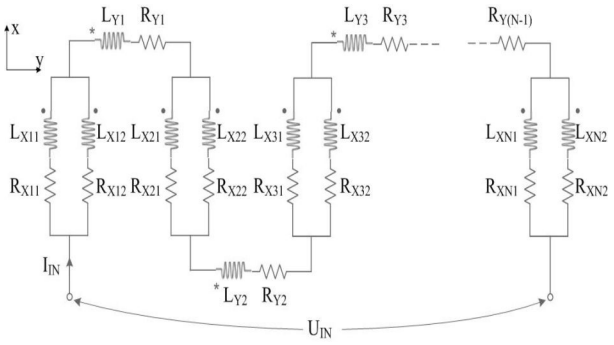

Figure 4: Equivalent circuit of the stationary coil with inserted gap in segments parallel to *x*-axis, l_x segments [13].

The input voltage U_{IN} is

$$\begin{aligned}\underline{U}_{IN} &= \underline{U}_{Rx11} + \underline{U}_{Lx11} + \underline{U}_{Rx21} + \underline{U}_{Lx21} + \ldots \\ &+ \underline{U}_{RxN1} + \underline{U}_{LxN1} + \underline{U}_{Ry1} + \underline{U}_{Ly1} + \\ &+ \underline{U}_{Ry2} + \underline{U}_{Ly2} + \ldots + \underline{U}_{Ry(N-1)} + \underline{U}_{Ly(N-1)}\end{aligned} \quad 3.1$$

Because of the coupling between bars, (2) follows:

$$\begin{aligned}\underline{U}_{Rx11} + \underline{U}_{Lx11} &= \big(R_{x11} + j\omega L_{x11} - j\omega M_{(11)(21)} + \\ &+ j\omega M_{(11)(31)} - \ldots\ldots - j\omega M_{(11)(N1)} + j\omega M_{(11)(12)} - \\ &- j\omega M_{(11)(22)} + \ldots\ldots - j\omega M_{(11)(N2)}\big) \cdot \frac{\underline{I}_0}{2}\end{aligned} \quad 3.2$$

where R_{xi1} is the resistivity of the left bar in l_{xi} segment, L_{xi1} is the partial self-inductance of the bar, $M_{(i1)(j1)}$ and $M_{(i1)(j2)}$ are the mutual inductances between bars, N is the number of l_x segments (N = 10). The mutual inductance between bars is positive if the current flows through the bars in the same direction and negative if the current flows through the bars in the opposite direction. Summing voltages in all segments, the input voltage U_{IN} is

$$\begin{aligned}\underline{U}_{IN} &= (R_{x11} + j\omega L_{x11} - j\omega M_{(11)(21)} + j\omega M_{(11)(31)} - \ldots - j\omega M_{(11)(N1)} + j\omega M_{(11)(12)} - \\ &- j\omega M_{(11)(22)} + \ldots - j\omega M_{(11)(N2)}) \cdot \frac{\underline{I}_{IN}}{2} + (R_{x21} + j\omega L_{x21} - j\omega M_{(21)(11)} - \\ &- j\omega M_{(21)(31)} + \ldots + j\omega M_{(21)(N1)} - j\omega M_{(21)(12)} + j\omega M_{(21)(22)} - \ldots + j\omega M_{(21)(N2)}) \cdot \frac{\underline{I}_{IN}}{2} + \\ &\vdots \\ &+ (R_{xN1} + j\omega L_{xN1} - j\omega M_{(N1)(11)} + j\omega M_{(N1)(21)} - \ldots - j\omega M_{(N1)((N-1)1)} - j\omega M_{(N1)(12)} + \\ &+ j\omega M_{(N1)(22)} - \ldots + j\omega M_{(N1)(N2)}) \cdot \frac{\underline{I}_{IN}}{2} + (R_{y1} + j\omega L_{y1} + j\omega M_{(y1)(y2)} + \\ &+ j\omega M_{(y1)(y3)} + \ldots + j\omega M_{(y1)(y(N-1))}) \cdot \underline{I}_{IN} + (R_{y2} + j\omega L_{y2} + j\omega M_{(y2)(y1)} + \\ &+ j\omega M_{(y2)(y3)} + \ldots + j\omega M_{(y2)(y(N-1))}) \cdot \underline{I}_{IN} + \\ &\vdots \\ &+ (R_{y(N-1)} + j\omega L_{y(N-1)} + j\omega M_{(y(N-1))(y1)} + j\omega M_{(y(N-1))(y2)} + \ldots + j\omega M_{(y(N-1))(y(N-2))}) \cdot \underline{I}_{IN}\end{aligned} \quad 3.3$$

Finally, it is obtained that the input impedance of the stationary coil with inserted gap (Figure 3) is

$$\underline{Z}_{IN} = \frac{\underline{U}_{IN}}{\underline{I}_{IN}} = \frac{1}{2}\underline{Z}_x + \underline{Z}_y, \quad 3.4$$

where Z_x is the impedance of the segments parallel to *x*-axis (l_x segments) and Z_y is the impedance of the segments parallel to *y*-axis (l_y segments).

The impedance Z_x is given by

$$\underline{Z}_x = \sum_{i=1}^{N}(R_{xi1} + j\omega(L_{xi1} + \sum_{\substack{j=1 \\ i\neq j}}^{N}(-1)^{i+j} M_{(i1)(j1)} + \\ + \sum_{j=1}^{N}(-1)^{i+j} M_{(i1)(j2)})) \quad 3.5$$

where R_{xi1} is the resistivity of the left bar in l_{xi} segment, L_{xi1} is the partial self-inductance of the bar, $M_{(i1)(j1)}$ and $M_{(i1)(j2)}$ are the mutual inductances between bars.

The impedance Z_y is given as

$$\underline{Z}_y = \sum_{i=1}^{N-1}(R_{yi} + j\omega(L_{yi} + \sum_{\substack{j=1 \\ i\neq j}}^{N-1} M_{(yi)(yj)})) \quad 3.6$$

where R_{yi} is the resistivity of l_y segments, $M_{(yi)(yj)}$ is the mutual inductance between l_y segments. The loop envelops the left bars of l_x segments, yet the same result is obtained if the loop envelops the right bars of l_x segments.

Further extension of the useful measurement range could be achieved with inserting more narrow gaps in each segment parallel to *x*-axis. However, the number of gaps and their width are the consequence of the chosen geometrical parameters and limitations of the chosen technology for sensor prototypes. The geometrical parameters of meander coils were determined as a compromise between the value of the inductance that could be measured by an electrical interface for signal processing and the size of the meander coils. The mathematical model, which describes influence of two gaps inserted in each segment parallel to *x*-axis, has been presented in Figure 5.

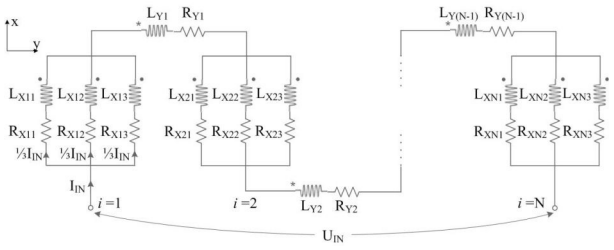

Figure 5: Equivalent circuit of the stationary coil with two inserted gaps in segments parallel to *x*–axis, l_x segments.

It was assumed that the current intensity in all bars was equal, and that phase shift did not change. The input voltage U_{IN} is:

$$\begin{aligned}\underline{U}_{IN} = (&R_{x11} + j\omega L_{x11} + j\omega M_{(11)(12)} + j\omega M_{(11)(13)} - j\omega M_{(11)(21)} - j\omega M_{(11)(22)} - j\omega M_{(11)(23)} + \\ &+ j\omega M_{(11)(31)} + j\omega M_{(11)(32)} + j\omega M_{(11)(33)} - j\omega M_{(11)(41)} - j\omega M_{(11)(42)} - j\omega M_{(11)(43)} + \\ &\vdots \\ &- j\omega M_{(11)(N1)} - j\omega M_{(11)(N2)} - j\omega M_{(11)(N3)}) \cdot \frac{\underline{I}_{IN}}{3} + (R_{y1} + j\omega L_{y1} + j\omega M_{(y1)(y2)} + j\omega M_{(y1)(y3)} + \\ &+ ... + j\omega M_{(y1)(yN-1)} + R_{y2} + j\omega L_{y2} + j\omega M_{(y2)(y1)} + j\omega M_{(y2)(y3)} + ... + j\omega M_{(y1)(yN-1)} + \\ &\vdots \\ &+ R_{yN-1} + j\omega L_{yN-1} + j\omega M_{(y1)(yN-1)} + + j\omega M_{(y2)(yN-1)} + ... + j\omega M_{(yN-1)(yN-2)}) \cdot \underline{I}_{IN}\end{aligned} \quad 3.7$$

Finally, it is obtained that the input impedance of the stationary coil with two inserted gaps is:

$$\underline{Z}_{IN} = \frac{\underline{U}_{IN}}{\underline{I}_{IN}} = \frac{1}{3}\underline{Z}_x + \underline{Z}_y, \quad 3.8$$

where Z_x is the impedance of the segments parallel to *x*-axes (l_x segments) and Z_y is the impedance of the segments parallel to *y*-axes (l_y segments).

The impedance Z_x is given as

$$\underline{Z}_x = \sum_{i=1}^{N}(R_{xi1} + j\omega L_{xi1} + j\omega \sum_{\substack{j=1 \\ i\neq j}}^{N}(-1)^{i+j} M_{(i1)(j1)} \cdot \\ + j\omega \sum_{j=1}^{N}(-1)^{i+j} M_{(i1)(j2)} + j\omega \sum_{j=1}^{N}(-1)^{i+j} M_{(i1)(j3)}) \quad 3.9$$

$$\underline{Z}_x = \sum_{i=1}^{N}(R_{xi1} + j\omega L_{xi1} + j\omega \sum_{j=1}^{N}(-1)^{i+j} M_{(i1)(j1)} + \\ + j\omega \sum_{j=1}^{N}\sum_{k=2}^{3}(-1)^{i+j} M_{(i1)(jk)} \quad 3.10$$

where R_{xi1} is the resistivity of a bar in l_x segment, L_{xi1} is the partial self-inductance of the bar, $M_{(i1)(j1)}$ and $M_{(i1)(jk)}$ are the mutual inductances between bars.

The impedance Z_y is given as

$$\underline{Z}_y = \sum_{i=1}^{N-1}(R_{yi} + j\omega L_{yi} + j\omega \sum_{\substack{j=1 \\ i\neq j}}^{N-1} M_{(yi)(yj)}) \quad 3.11$$

where R_{yi} is the resistivity of l_y segments, $M_{(yi)(yj)}$ is the mutual inductance between l_y segments.

3.2 Calculation of the self-inductances of the coils L_1 and L_2

The sensor was modeled using the concept of the partial inductance. Planar meander-type coils were partitioned into constituent segments. Each partitioned segment was partitioned additionally into a certain number of filaments [13, 14]. Planar meander coils are partitioned into constituent conductive segments as it is shown in Figure 6. There are 19 conductive segments in meander coils.

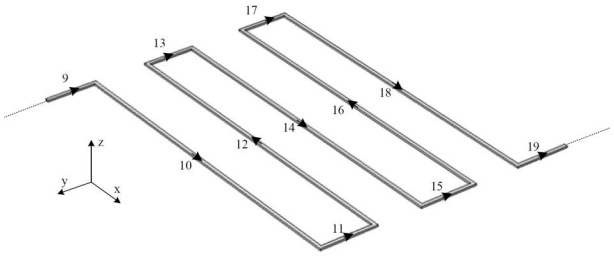

Figure 6: Arrows show current flow direction in the coil.

The resistances R_1 and R_2 of Coils 1 and 2, respectively, are calculated by Equations 3.12 and 3.13

$$R_1 = \sum_{i=1}^{h} R_i \qquad 3.12$$

$$R_2 = \sum_{i=1}^{h} R_i \qquad 3.13$$

where h is the number of segments in a coil (h = 19), and R_i is the resistance of a segment (parallel to x- or y-axes).

The resistance R_i is given by Equation 3.14

$$R = \rho_{Cu} \cdot \frac{l}{w \cdot t} \qquad 3.14$$

where ρ_{Cu} is resistivity of copper, l is the length of the segment, w is the width of the segment and t is the thickness of the segment (copper layer).

The self-inductances of meander Coils 1 and 2 (L_1 and L_2) can be calculated as a sum:

$$L_2 = \sum_{i=1}^{h} L_i \pm \sum_{\substack{i=1 \\ j \neq i}}^{h} \sum_{j=1}^{h} \left| M_{ij} \right| \qquad 3.15$$

$$L_2 = \sum_{i=1}^{h} L_i \pm \sum_{\substack{i=1 \\ j \neq i}}^{h} \sum_{j=1}^{h} \left| M_{ij} \right| \qquad 3.16$$

where L_i is the partial self-inductance of each straight segment (Figure 6) and M_{ij} is the mutual inductance between each pair of conductive segments (Figure 6), h is the number of partitioned segments in meander coils (h = 19). The mutual inductance is positive if current vectors in segments i and j are in the same direction or negative if current vectors are in opposite directions.

As it was reported in [16, 17], each partitioned segment was additionally partitioned into a certain number of elementary filaments (l_{1Xi}, l_{1Yi}, l_{2Xj}, l_{2Yj},…), having small, rectangular cross sections, as shown in Figure 7. This was done in order to achieve better precision in calculation, because the segment separation dimensions are not larger than the cross sectional dimensions for all geometries considered. (As it was previously reported, the distance between axis of two neighboring segments is p = 1.78 mm whereas, in one of the structures, cross sectional dimension is 1.52 mm.) Figure 7 shows the general case of segments partitioning, with overlapping in the corners. In reality, dimensions of the overlapping in the corners are too small to introduce significant error.

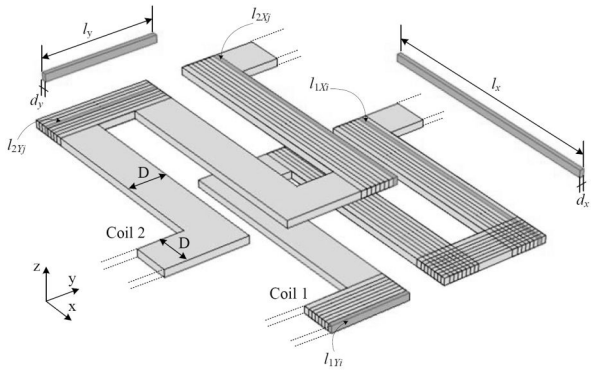

Figure 7: A part of sensor element partitioned into filaments. Filaments parallel to x-axis are l_x long and d_x wide, whereas filaments parallel to y-axis are l_y long and d_y wide; D is the width of conductive segments.

The number of filaments is such that dimensions of the cross section of each filament are less than a skin depth ($\delta = \sqrt{\rho_{Cu} / \pi f \mu_0}$, where ρ_{Cu} = 1.72 × 10^{-8} Ω is electrical resistivity of copper *Cu*, f the working frequency and $\mu_0 = 4\pi \times 10^{-7}$ H/m the permeability), at the highest frequency of interest [17]. Each segment was partitioned into 24 filaments as to fulfill this condition and as compromise between complexity and accuracy of the model.

The partial self-inductance L_i is the sum of the mutual inductances between all pairs of elementary filaments within segment i:

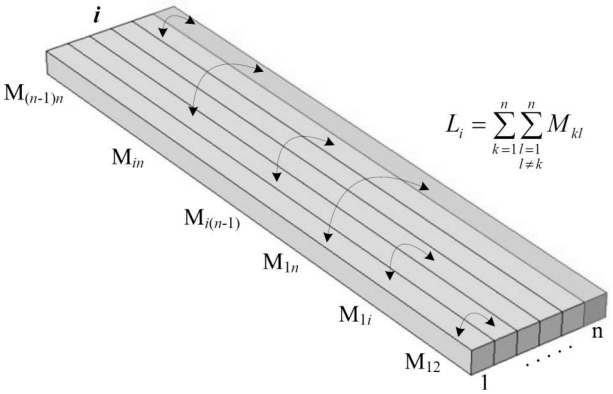

Figure 8: The partial self-inductance calculation of a conductive segment i.

$$L_i = \sum_{k=1}^{n} \sum_{\substack{l=1 \\ l \neq k}}^{n} M_{kl} \qquad 3.17$$

where n is the number of filaments in segment i and M_{kl} is the mutual partial inductance between filaments k and l within segment i, as it is shown in Figure 8.

The mutual inductance M_{ij} (Equations 3.15 and 3.16) is the sum of mutual inductances between all pairs of filaments from segments i and j:

$$M_{ij} = \frac{1}{m_1 \cdot m_2} \sum_{k=1}^{m_1} \sum_{l=1}^{m_2} M_{kl} \qquad 3.18$$

where m_1 and m_2 are the number of filaments in segments i and j, respectively, and M_{kl} is the mutual inductance between filaments k and l from segments i and j, as it is shown in Figure 9. The numbers of filaments in conductive segments are identical, $n = m_1 = m_2 = 24$.

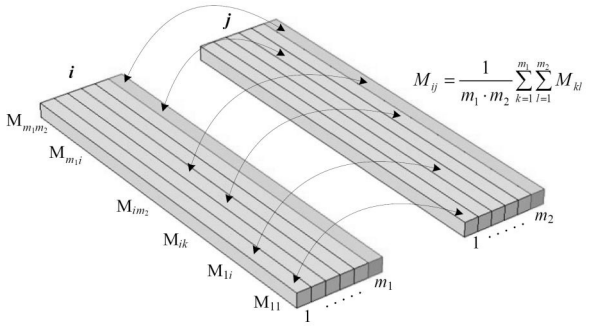

Figure 9: The mutual inductance calculation between two segments.

3.3 The mutual inductance M_{12} calculation

The mutual inductance between Coils 1 and 2 (M_{12}) is calculated in a similar manner, as it is presented in Figure 10.

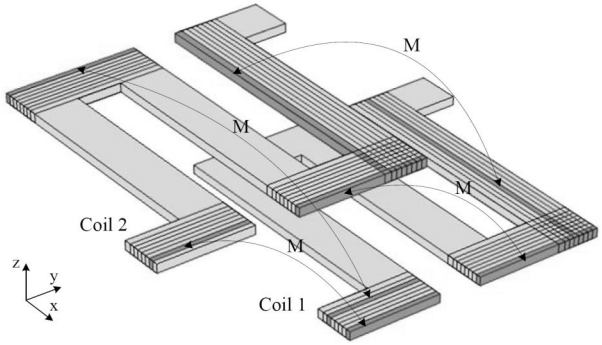

Figure 10: Mutual inductance M_{12} calculation.

The mutual partial inductance is calculated between each pair of elementary filaments, which belong to different coils. M_{12} is the sum of all mutual partial inductances between filaments from Coils 1 and 2. Taking into account, that Coil 2 physically moves with respect to Coil 1, the distance between filaments of Coils 1 and 2 changes regarding the displacement. The distance between filaments is an important parameter for the mutual inductance calculation, as well their mutual position. While calculating the mutual partial inductances between filaments from different coils different equations were applied [18], depending on the mutual position between filaments, as it can be seen in Figure 11. The formula for mutual inductance of two parallel filaments of equal length (l) and distance (d) is

$$M = M(l,d) = \frac{\mu}{2\pi} l \left[\ln\left(\frac{l}{d} + \sqrt{1 + \frac{l^2}{d^2}} \right) - \sqrt{1 + \frac{d^2}{l^2}} + \frac{d}{l} \right] \qquad 3.19$$

In the model of the sensor, Coil 2 moves with respect to Coil 1 in y-z plane and it rotates around x- and y- axis, as well. In the case of rotation, filaments in Coil 2 can be placed in any desired position. Therefore, equations 3.20 – 3.22 [18] were applied to calculate the mutual partial inductance between filaments placed in any desired position, as it is shown in Figure12. Based on this model of the sensor, in-house software was specifically developed for resistance, inductance, and impedance calculation of the sensor. The software calculates variation of these parameters versus displacement in y-z plane and versus small rotations of the moving coil around x- and y-axes.

$$\frac{M}{0.01\cos\varepsilon} = 2[(\mu+1) \cdot arctg\frac{m}{R_1+R_2} + (v+m) \cdot arctg\frac{l}{R_1+R_4} - \mu \cdot arctg\frac{m}{R_3+R_4} - v \cdot arctg\frac{l}{R_2+R_3}] - \frac{\Omega d}{\sin\varepsilon} \qquad 3.20$$

in which

$$\Omega = arctg\left\{\frac{d^2\cos\varepsilon + (\mu+l)(v+m)\sin^2\varepsilon}{dR_1\sin\varepsilon}\right\} - arctg\left\{\frac{d^2\cos\varepsilon + (\mu+l)v\sin^2\varepsilon}{dR_2\sin\varepsilon}\right\} + arctg\left\{\frac{d^2\cos\varepsilon + \mu v\sin^2\varepsilon}{dR_3\sin\varepsilon}\right\} - arctg\left\{\frac{d^2\cos\varepsilon + \mu(v+m)\sin^2\varepsilon}{dR_4\sin\varepsilon}\right\} \qquad 3.21$$

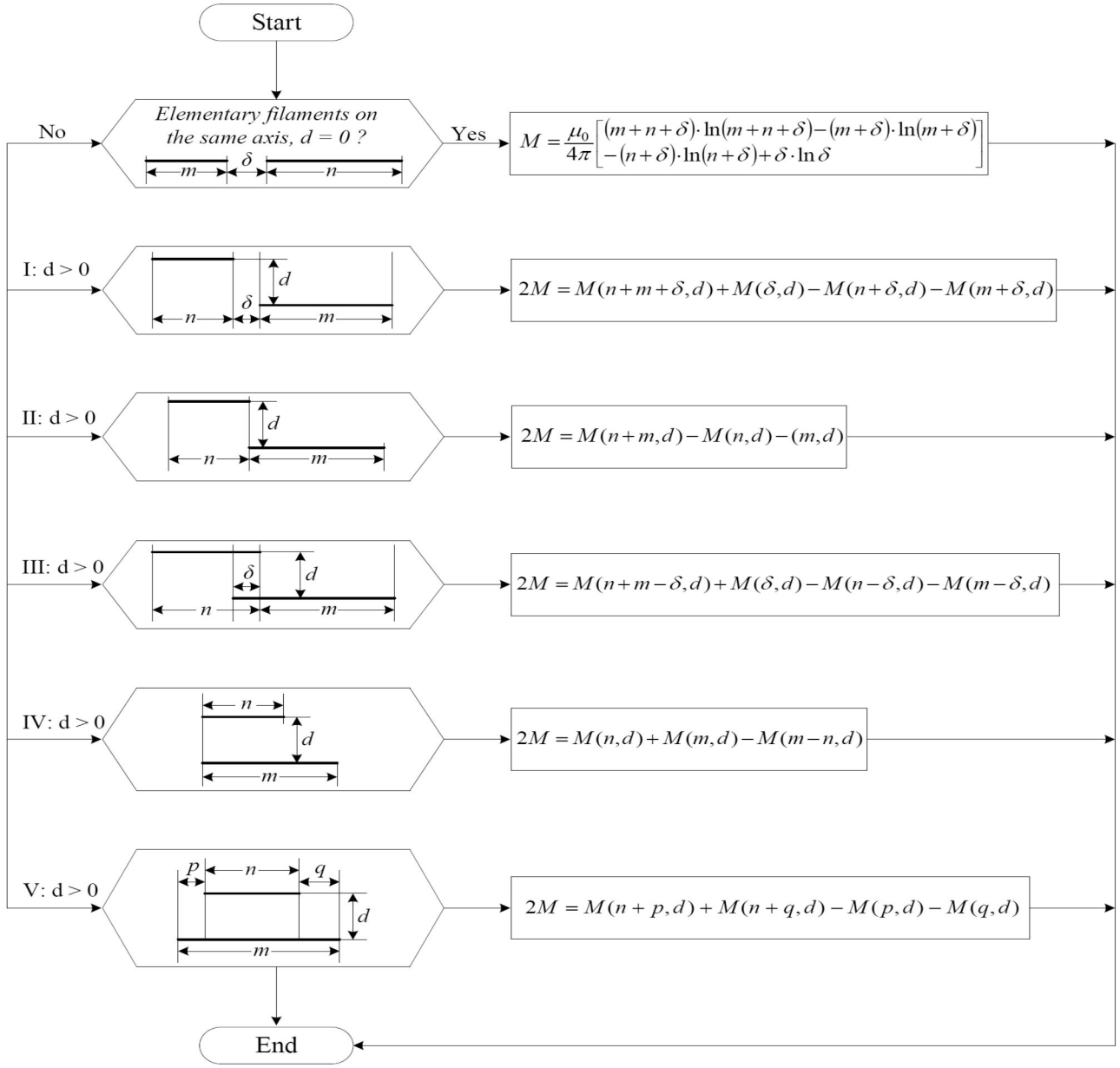

Figure 11: Calculation of the mutual inductance between filaments. Calculation depends on the mutual position between filaments.

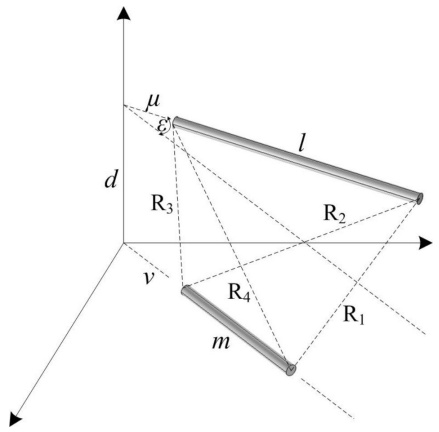

Figure 12: Two filaments placed in any desired position.

Parameters *l*, *m*, *μ*, *v*, and *d* are given. The relations 3.22 calculate the distances R_1, R_2, R_3, and R_4

$$\begin{aligned} R_1^2 &= d^2+(\mu+l)^2+(v+m)^2-2(\mu+l)(v+m)\cos\varepsilon \\ R_2^2 &= d^2+(\mu+l)^2+v^2-2v(\mu+l)\cos\varepsilon \\ R_3^2 &= d^2+\mu^2+v^2-2\mu v\cos\varepsilon \\ R_4^2 &= d^2+\mu^2+(v+m)^2-2\mu(v+m)\cos\varepsilon \end{aligned} \qquad 3.22$$

4 Results and Discussion

Simulated values of the input inductance versus *y*-displacement for different gap widths *g* = [0.15, 0.18,

0.20, 0.23, 0.25, 0.28, 0.30, 0.33, 0.36, 0.38] mm and the most critical normal distance between coils $z = 0.1$ mm are presented in Figure 13. It can be observed in Figure 13, that invariance of the input inductance versus *y*-displacement near $y = 0$ is obtained for gaps g =0.23 mm red line, $g = 0.25$ mm blue line, and $g = 0.28$ mm green line. The input inductance changes versus tangential displacement if the gap width is increased above 0.28 mm. If the gap width is decreased below 0.23 mm, then the useful measurement range is narrower, as it can be seen in Figure 13. The variation of the input inductance versus *y*-displacement for gap widths $g = 0.23$ mm (red solid line), $g = 0.25$ mm (blue dash line), and $g = 0.28$ mm (green dot line) is presented in Figure 14. It can be seen that there is a slight variation of the input inductance in the useful measurement range (near $y = 0$) for gap widths $g = 0.25$ mm and $g = 0.28$ mm. Thus, it was chosen that the optimal useful measurement range was obtained for gap width $g = 0.23$ mm. The gap width $g = 0.23$ mm provides invariance of the input inductance versus tangential displacement in the useful measurement range, thus making sensor element good for detecting normal displacement.

The sensor element for detecting normal displacement with the gap width $g = 0.23$ mm was fabricated, characterized, and compared with the sensor element without the gap. Fabricated prototypes are presented in Figure 15. Sensor prototypes were electrically tested by Impedance Analyzer HP4194A, at the working frequency of 1 MHz. Characterization procedure is similar as it was described in [19].

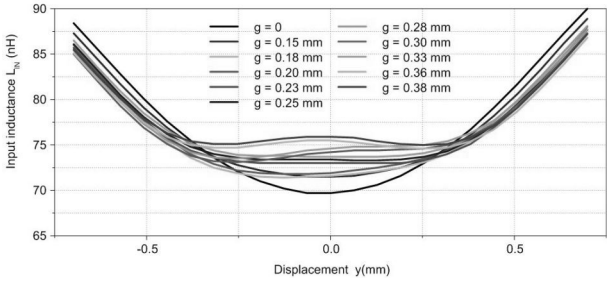

Figure 13: The sensor element that detects normal displacement: Simulated values of the input inductance variation versus y-displacement for different gap widths, and the most critical normal distance between the coils $z = 0.1$ mm.

The displacement dependence of the input inductance L_{IN} in *y-z* plane for the sensor element detecting normal displacement without the gap is presented in Figure 16 and with the gap $g = 0.23$ mm in Figure 17. The symmetry and periodicity of the input inductance characteristics can be observed in Figures 16 and 17. The difference between local minimums (L_{INmin}) and maximums

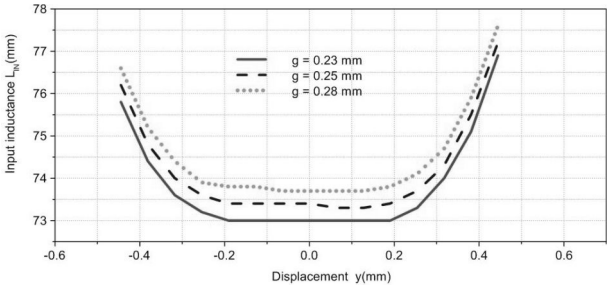

Figure 14: The sensor element that detects normal displacement: Simulated values of the input inductance variation versus *y*-displacement for gap widths $g = 0.23$ mm, $g = 0.25$ mm, and $g = 0.28$ mm, and the most critical normal distance between the coils $z = 0.1$ mm.

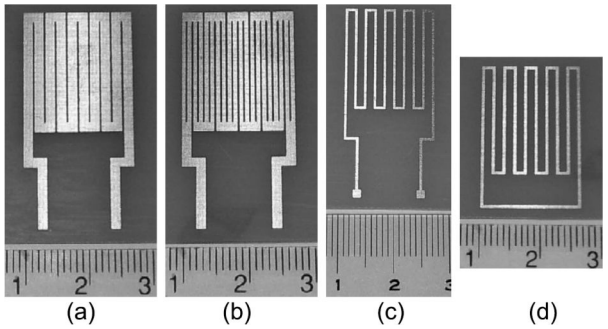

Figure 15: The sensor element: a) The stationary coil of sensor element that detects normal displacement without the gap, b) The stationary coil with inserted gap $g = 0.23$ mm, c) The stationary coil of sensor element that detects tangential displacement, and c) The moving (short-circuited) coil.

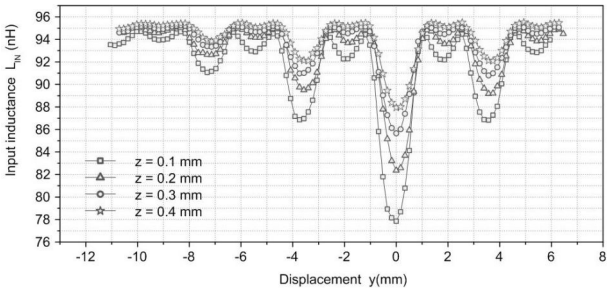

Figure 16: The sensor element detecting normal displacement: The displacement dependence of the input inductance L_{IN} in *y-z* plane.

(L_{INmax}) decreases as the moving coil moves from the stationary coil in *y-z* plane. Eventually, the tendency of the input inductance characteristic is to achieve the self-inductance of the stationary coil. Figures 16 and 17 present displacement-input inductance dependence in the nearly whole *y*-displacement range. However, the useful measurement range is near $y = 0$ for sensor element detecting normal displacement.

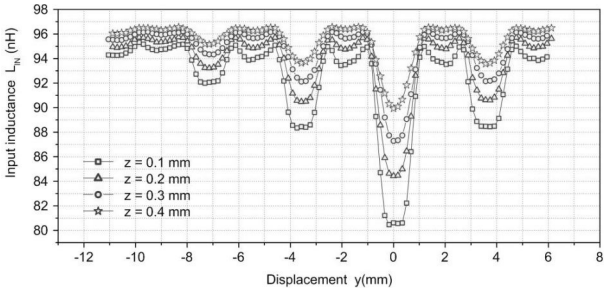

Figure 17: The sensor element detecting normal displacement with inserted gap g = 0.23 mm: The displacement dependence of the input inductance L_{IN} in *y-z* plane.

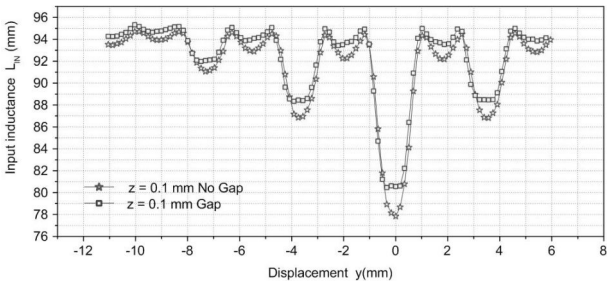

Figure 18: The sensor element detecting normal displacement without the gap and with the gap g = 0.23 mm: The displacement dependence of the input inductance L_{IN} in *y-z* plane.

Comparison of the input inductance characteristic L_{IN} for the sensor element detecting normal displacement without the gap and with the gap, for the most critical normal distance between the coils z = 0.1 mm, is presented in Figure 18. It can be observed that the invariance of the input inductance versus *y*-displacement is achieved in the useful measurement range (near y = 0), as well near other local minimums. Comparison of the useful measurement range between the sensor elements without the gap and with the gap is presented in Figure 19. Displacement step was approximately 0.0635 mm as to accurately analyze the useful measurement range. It can be seen in Figure 19, that the input inductance of the sensor element with the inserted gap is almost invariant near y = 0 in comparison with the input inductance of the sensor element without the gap.

The smallest change in the position of a moving coil that can be detected depends on the signal processing interface. In case of measuring with Impedance analyzer, which can detect transition in the range of 10 micro ohms, resolution of the sensor can be estimated to 0.1 μm. Further, resolution of the sensor is possible to improve with adjusting the design to meet the given applications. The useful measurement range of the sensor element detecting normal displacement, the worst-

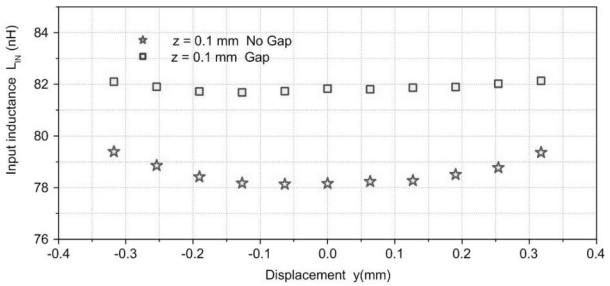

Figure 19: Comparison of the useful measurement ranges for the sensor element without the gap and with the gap g = 0.23 mm when displacement step was 0.0635 mm and for the most critical normal distance between coils z = 0.1 mm.

case results for g = 0, is nearly 0.31 mm for relative accuracy ±0.5%, and nearly 0.42 mm for relative accuracy ±1%. From Figure 19, it could be observed that these ranges would be wider for the optimal useful measurement range g = 0.23 mm and for given accuracies.

5 Conclusion

In this paper, concept of the partial inductance was used as to model a planar displacement sensor with inductive coils of meander-type. In addition, modeling of a gap, inserted in a meander coil, was presented as well. In-house software was developed, based on this model, and was used to determine numerically the optimal useful measurement range of the sensor. Results show that for the sensor with specific geometrical parameters, as it is given in the paper, the optimal useful measurement range is obtained if the gap of 0.23 mm is inserted in the stationary coil. Theoretical predictions were confirmed with experimental results.

6 Acknowledgment

This work was supported by the Ministry of Education, Science, and Technological Development, Serbia, under Grant TR32016 and Grant III45021.

7 References

1. Yamada, S., Nakamura, K., Iwahara, M., Taniguchi, T., and Wakiwaka, H., "Application of ECT technique for inspection of bare PCB", *IEEE Transactions on Magnetics*, Vol. 39, No. 5, pp. 3325-3327, 2003.
2. Chomsuwan, K., Yamada, S., and Iwahara, M., "Improvement of defect detection performance of PCB

inspection based on ECT technique with multi-SV-GMR sensor", Vol. 43, No. 6, pp. 2394-2396, 2007.
3. Bayani, H., Nishino, M., Yamada, S., and Iwahara, M., "Introduction of a base model for eddy-current testing of printed circuit boards", *IEEE Transactions on Magnetics*, Vol. 44, No. 11, pp. 4015-4017, 2008.
4. Baschirotto, A., Dallago, E., Malcovati, P., Marchesi, M., and Venchi, G., "Development and comparative analysis of fluxgate magnetic sensor structures in PCB technology", *IEEE Transactions on Magnetics*, Vol. 42, No. 6, pp. 1670-1680, 2006.
5. Cha, Y.-J., Nam, B., Kim, J., and Kim, K. H., "Evaluation of the planar inductive magnetic field sensors for metallic crack detections", *Sensors and Actuators A: Physical*, Vol. 162, No. 1, pp. 13-19, 2010.
6. Norhisam, M., Norrimah, A., Wagiran, R., Sidek, R. M., Mariun, N., and Wakiwaka, H.,
7. "Consideration of theoretical equation for output voltage of linear displacement sensor using meander coil and pattern guide", *Sensors and Actuators A: Physical*, vol. 147, No. 2, pp. 470–473, 2008.
8. Misron, N., Ying, L. Q., Firdaus, R. N., Abdullah, N., Mailah, N. F., and Wakiwaka, H., "Effect of inductive coil shape on sensing performance of linear displacement sensor using thin inductive coil and pattern guide", *Sensors*, Vol. 11, No. 11, pp. 10522-10533, 2011.
9. Wang, H., and Feng, Z., "Ultrastable and highly sensitive eddy current displacement sensor using self-temperature compensation", *Sensors and Actuators A: Physical*, Vol. 203, pp. 362-368, 2013.
10. Jerance, N., Bednar, N., and Stojanovic, G., "An ink-jet eddy current position sensor", *Sensors*, Vol. 13, No. 4, pp. 5205-5219, 2013.
11. Laskoski, G. T., Pichorim, S. F., and Abatti, P. J., "Distance measurement with inductive coils", *IEEE Sensors Journal*, Vol. 12, No. 6, pp. 2237-2242, 2012.
12. Yunus, M. A. Md., and Mukhopadhyay S. C., "Novel planar electromagnetic sensors for detection of nitrates and contamination in natural water sources", *IEEE Sensors Journal*, Vol. 11, No. 6, pp. 1440-1447, 2011.
13. Yunus, M. A. Md., and Mukhopadhyay, S. C., "Development of planar electromagnetic sensors for measurement and monitoring of environmental parameters", *Measurement Science and Technology*, Vol. 22, No. 2, 025107 (9pp), 2011.
14. Damnjanovic, M. S., Zivanov, Lj. D., Nagy, L. F., Djuric, S. M., and Biberdzic, B. N., "A novel approach to extending the linearity range of displacement inductive sensor", *IEEE Transactions on Magnetics*, Vol. 44, No. 11, pp. 4123-4126, 2008.
15. Djuric, S. M., Nagy, L. F., Damnjanovic, M. S., Djuric, N. M., and Zivanov, Lj. D., "A novel application of planar-type meander sensors", *Microelectronics International*, Vol. 28, No. 1, pp. 41–49, 2011.
16. Wakiwaka, H., Nishizawa, H., Yanase, S., Maehara, O., "Analysis of impedance characteristics of meander coil", *IEEE Transactions on Magnetics*, Vol. 32, No. 5, pp. 4332-4334, 1996.
17. Ruehli, A. E., "Inductance calculations in a complex integrated circuit environment," *IBM Journal of Research and Development*, Vol. 16, No. 5, pp. 470 – 481, 1972.
18. Ruehli A., Paul C., and Garett, J., "Inductance calculations using partial inductances and macromodels" *Proceedings of the International Symposium on EMC*, Atlanta, USA, pp.23-27, 1995.
19. Grover, F. W., *Inductance calculation*, D. Van Nostrand Company, New York, 1946.
20. Djuric, S. M., "Performance analysis of a planar displacement sensor with inductive spiral coils", *IEEE Transactions on Magnetics*, Vol. 50, No. 4, 4004104 (4pp), 2014.

Arrived: 04. 01. 2015
Accepted: 06. 03. 2015